Ultrafast Science
A SCIENCE PARTNER JOURNAL

RESEARCH ARTICLE

# Optical Measurement of Photorecombination Time Delays

**Chunmei Zhang[1,2*†], Graham Brown[1,3*†], Dong Hyuk Ko[1], and P. B. Corkum[1]**

[1]Joint Attosecond Science Laboratory, University of Ottawa and National Research Council of Canada, 25 Templeton St, Ottawa, ON K1N 6N5, Canada. [2]Beijing Institute of Technology, No. 5, South Street, Zhongguancun, Haidian District, Beijing, China. [3]Max Born Institute, Max Born Str. 2a, 12489 Berlin, Germany.

*Address correspondence to: chunmei.zhang@bit.edu.cn (C.Z.); graham.brown@uottawa.ca (G.B.)
†These authors contributed equally to this work.

Recollision physics and attosecond pulse generation meld the precision of optics with collision physics. As a follow-up to our previous work, we reveal a new direction for the study of electronic structure and multielectron dynamics by exploiting the collision-physics nature of recollision. We show experimentally that, by perturbing recollision trajectories with an infrared field, photorecombination time delays can be measured entirely optically using the Cooper minimum in argon as an example. In doing so, we demonstrate the relationship between recollision trajectories and the transition moment coupling the ground and continuum states. In particular, we show that recollision trajectories are influenced by their parent ion, while it is commonly assumed they are not. Our work paves the way for the entirely optical measurement of ultrafast electron dynamics and photorecombination delays due to electronic structure, multielectron interaction, and strong-field-driven dynamics in complex molecular systems and correlated solid-state systems.

**Citation:** Zhang C, Brown G, Ko DH, Corkum PB. Optical Measurement of Photorecombination Time Delays. *Ultrafast Sci.* 2023;3:Article 0034. https://doi.org/10.34133/ultrafastscience.0034

Submitted 4 November 2022
Accepted 5 June 2023
Published 7 August 2023





## Introduction

Recollision consists of 3 steps [1]: (a) in the presence of a strong field, an electron tunnels into the continuum (ionization), (b) the electron is accelerated by the strong field (propagation), and (c) the electron recombines with its parent ion and emits an attosecond pulse (recombination). The spectral phase of attosecond pulses generated through recollision is predominantly shaped by the field-driven continuum dynamics during the propagation step [2,3], but can be shaped by the phase of the transition moment coupling the ground and continuum states during tunnel ionization or recombination [4]. Thus, the measurement of the spectral phase of attosecond pulses can reveal information about the underlying structure of the generation medium through the characterization of the transition moment phase.

The measurement of the spectral phase of attosecond pulses is most commonly accomplished by photoionizing a target atom with an attosecond pulse in the presence of a weak infrared field [5–7]. In this regime, known as attosecond ex situ measurement, the phase of the attosecond pulse and, thus, the transition moment of the generation atom are imprinted onto the photoelectron spectrum from the target atom and this can be measured by monitoring the variation of the photoelectron spectrum with the delay between the attosecond pulse and infrared field.

An experimentally simpler alternative form of attosecond measurement was first proposed in 2006 [8] and involves the perturbation of the recollision process, which generates an attosecond pulse with a weak infrared field. As the delay between the weak infrared field and the field driving recollision is varied, the attosecond pulse intensity spectrum varies and this variation can be used to measure the spectral phase of the recollision electron up to a constant [8–11]. This form of measurement, referred to in situ or all-optical measurement, has been applied to several gas-phase high harmonic generation (HHG) experiments extended to solid-state HHG [12] and has become an invaluable tool for the characterization of recollision dynamics [13–16]. Previous works [16,17], however, have demonstrated that these all-optical techniques are insensitive to transition moment phase shifts arising from 2-center interference [17] and the recollision-induced excitation of a shape resonance [16]. Generally, it has been assumed that all-optical attosecond measurement is insensitive to the transition moment phase and only characterizes the dynamics of the recollision electron in the continuum [9].

The insensitivity of all-optical measurement to the transition moment phase follows from the assumption that the transition moment phase plays no role in determining recollision trajectories. Quantitative rescattering theory (QRS) [18] formalized this assumption and describes attosecond pulse spectra as the product of a universal continuum electron wave packet, specific

to the generation medium only through the ionization dynamics, and the field-free transition moment of the generation atom in the spectral domain. QRS suggests a means for the efficient calculation of HHG from complex systems with sufficient accuracy [19,20], and the mathematical formalism of QRS has reinforced the notion that recollision trajectories are independent of the transition moment phase.

In a recent work [21], we argued that this assumption is incorrect and argued that the transition moment does play a role in the determination of recollision trajectories. The implication of this is that all-optical measurement should be sensitive to the transition moment phase, which appears to conflict with the findings of previous works that demonstrated otherwise [16,17]. This work constitutes an experimental follow-up to our previous work [21], conclusively demonstrates the sensitivity of attosecond all-optical measurement to the transition moment phase, and confirms that the transition moment phase plays a role in the determination of recollision trajectories. To do this, we perform an attosecond all-optical measurement in argon, which exhibits a well-known Cooper minimum [22] and corresponding $\pi$-phase jump in its photorecombination cross-section. Our experimental results conclusively show that all-optical techniques are sensitive to the transition moment phase shift around the Cooper minimum in argon. We support these experimental findings using both ab initio simulations based on time-dependent density functional theory (TD-DFT) and an extension of the strong field approximation (SFA), the semiclassical model of recollision, which incorporates the transition moment phase [21]. The implications of our results are critically important for the interpretation and design of experimental attosecond measurement and has implications regarding the description of attosecond pulse generation on a fundamental level.

## Experimental Design

We begin by describing our experimental all-optical measurement and present the measured attosecond pulse spectral intensity and group delay alongside a simulation of the experimental conditions calculated using TD-DFT [23]. Our experimental measurement of the group delay variation around the Cooper minimum agrees with the simulation of experimental conditions. We then validate our interpretation of the experimental results by simulating perturbed attosecond pulse emission in argon using our theoretical model. We first show the difference in the spectral phase between perturbed and unperturbed attosecond pulse emission, demonstrating that the perturbation-induced phase shift is sensitive to the transition moment phase. We then present the results of a simulated optical measurement, which agrees with our experimental results. Finally, we present a physical interpretation of how the Cooper minimum affects recollision trajectories based on the semiclassical description of recollision known as the SFA [3].

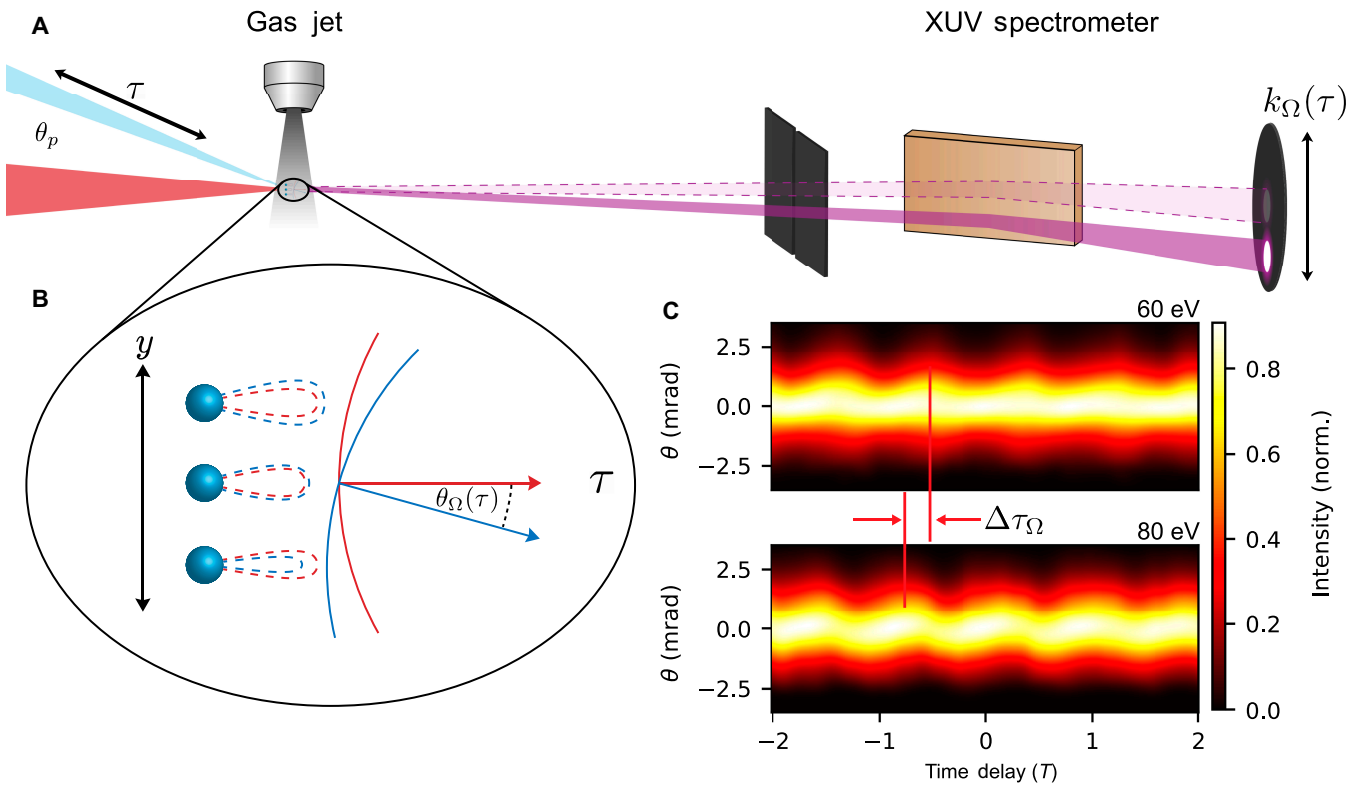


**Fig. 1.** Experimental diagram. (A) The polarization-gated driving pulse (red) and perturbing pulse delayed by time $\tau$ (blue) are focused into an argon gas jet. The perturbing pulse has a relative intensity less than $10^{-4}$ and incident angle of $\theta_p = 6.9$ mrad with respect to the driving field. (B) The perturbation induces a delay-dependent modulation of the electron trajectories and XUV wavefronts (red to blue) across the driving field beam front. This results in a deflection of the XUV beam in the far-field by a delay-dependent angle $\theta_\Omega(\tau)$, which is recorded in the XUV spectrometer. (C) The deflection of the XUV emission is recorded over a range of delays (in units of the perturbing field period $T_p$) and spectrally resolved. The resultant spectrograms for XUV energies of 60 (top) and 80 (bottom) eV are shown. The phase difference in the deflection modulation phase is proportional to the difference in group delay, $\Delta\tau_\Omega$, between the 2 energies.

For our experiment, we generate an isolated attosecond pulse in argon using polarization gating [24], which involves superposing left and right circularly polarized pulses separated by a small time delay. This results in a linear polarization within the temporal window where the 2 polarizations overlap. Since recollision is extremely sensitive to the ellipticity of the driving field [25], attosecond pulse emission is confined to this overlap region, resulting in the emission of an isolated attosecond pulse.

The experimental diagram of our all-optical measurement is shown in Fig. 1A. For more experimental details, please see the Supplementary Materials. We focus a 12 fs, polarization-gated driving pulse with a central wavelength of 1.8 μm into an argon gas jet, as shown by the red pulse. We perturb recollision with a second harmonic of the driving pulse delayed by a time $\tau$ that is polarized parallel to the linearly polarized component of the driving field, has a relative intensity less than $2 \times 10^{-4}$ (our procedure for estimating the ratio is discussed in the Supplementary Materials), and is focused into the gas jet at an angle of $\theta_p = 6.9$ mrad with respect to the driving beam. This is depicted by the blue beam in Fig. 1A. In the gas jet, the perturbing field modifies the recollision trajectories and imparts a phase shift that depends on the time delay between the driving and perturbing fields and the vertical position of the atom within the gas jet due to the noncollinear geometry.

The phase shift induced by the perturbing field can be calculated using the SFA as follows:

$$\sigma(k, t_b, t_r, \phi) = \int_{t_b}^{t_r} [k + A(\tau)] A_p(\tau, \phi) d\tau + A_p(t_b, \phi)\eta(k + A(t_b)) - A_p(t_r, \phi)\eta(k + A(t_b)), \quad (1)$$

where $k$ is the continuum electron canonical momentum, $t_b$ is the time of ionization, $t_r$ is the time of recombination, $A(t)$ and $A_p(t, \phi)$ are the driving and perturbing field vector potentials at time $t$ and relative phase $\phi$, and $\eta'(k)$ is the gradient of the transition moment phase for continuum state momentum $k$. A full description of the perturbation-induced phase shift is included in the Supplementary Materials, and vector notation has been omitted due to the assumption of a linearly polarized field. For our measurement, the relative phase $\varphi$ between the driving and perturbing field is determined from the time delay between the driving and perturbing fields, the vertical position within the gas jet, and the angle between the driving and perturbing beams [9].

As the time delay between the perturbing and driving fields is varied, the phase shifts of recollision trajectories across the driving field beam front change. This results in a varying far-field angular deflection of each spectral component of the extreme ultraviolet (XUV) emission, which we label as $\theta_\Omega(\tau)$. The difference in the phase of this modulation between 2 energies is proportional to the difference in XUV emission time [9]. This is depicted in Fig. 1C, which shows the resultant spectrograms for photon energies of 60 (top) and 80 eV (bottom). The difference in the modulation phase is proportional to the difference in emission times $\Delta\tau_\Omega$ for these energies. We have similar spectrograms for each frequency component. We record 200 attosecond pulse spectra for each delay step to reduce the influence of noise and fluctuations on the measurement. We then group the scans into 4 individual measurements, which we analyze separately to obtain the measured uncertainty.

## Results and Discussion

The emission time analysis is performed for each spectral component of the measured attosecond pulse, providing a measurement of the difference in emission time for each spectral component. The group delay of the recollision electron is obtained from the relative delay of each spectral component with respect to that of a fixed energy. Our experimental results and uncertainty are depicted in Fig. 2 by the solid red lines and shaded red regions in all subfigures, respectively. The unperturbed attosecond pulse spectrum is shown in Fig. 2A in red, where the Cooper minimum is observed near 54 eV. Based on the cutoff XUV photon energy of 110 eV, the pulse reaches a peak intensity of $1 \times 10^{14}$ W/cm$^2$ within the jet. The attosecond pulse spectrum calculated using a TD-DFT simulation of the unperturbed experimental conditions is shown by the dashed line (scaled ×10 for clarity). Absorbing boundaries [26] are used beginning at a radius of $F_0 / \omega_0^2$ to suppress long trajectory emission, where $F_0$ is the peak electric field amplitude and $\omega_0$ is the driving field frequency. The position of the Cooper minimum in the TD-DFT simulation, near 51 eV, is lower than the experimental result, near 54 eV. The positions of the Cooper

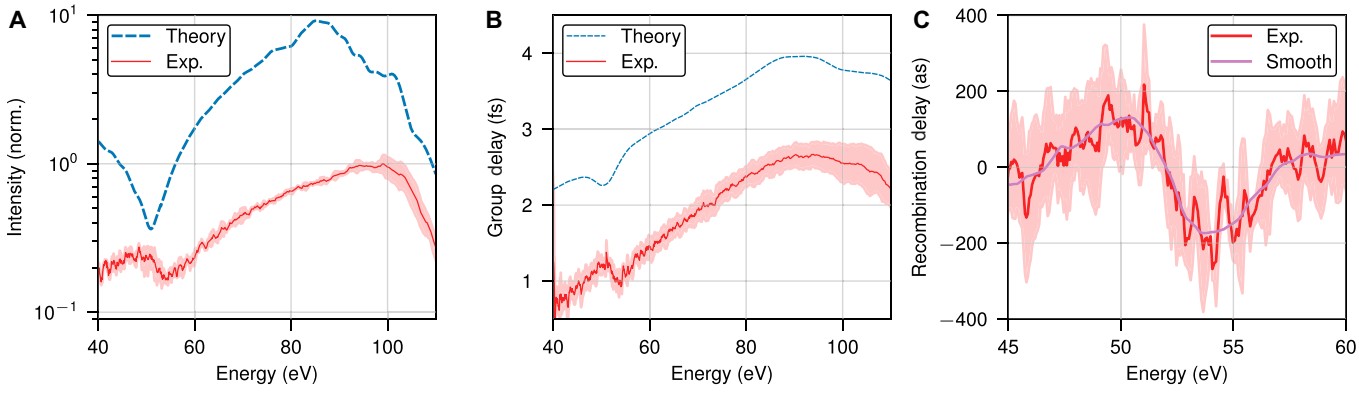


**Fig. 2.** Experimental all-optical measurement in argon. (A) Measured intensity spectrum and (B) group delay for the attosecond pulse generated in argon (solid line) by a 12 fs 1.8 μm driving field with a peak intensity of $1 \times 10^{14}$ W/cm$^2$. The dashed lines show the spectrum and group delay from a TD-DFT simulation of the experimental conditions. (C) Difference between the measured group delay and the expected semiclassical result in the spectral region of the Cooper minimum before (red) and after (magenta) smoothing the data. The shaded red region denotes the experimental uncertainty.

minimum from our simulation and experiment, however, both agree with previously published theoretical [27,28] and experimental results [29]. Given the message of this work concerns the qualitative capabilities of all-optical attosecond measurement, it only is the qualitative dynamics of recollision and the effect of the Cooper minimum on recollision trajectories that are important for our work. We use a thin gas jet to minimize the macroscopic contributions due to phase matching and placed the jet before the beam focus.

The measured group delay is shown in Fig. 2B, where the experimental data are shown as a solid red line and the group delay from our TD-DFT simulation of the experimental conditions is shown by a dashed line with a vertical offset for clarity. Both the experimental and theoretical group delay curves are predominantly linear until the cutoff energy near 90 eV, but deviate from linearity near the Cooper minimum. The difference between the experimentally measured group delay and the linear group delay expected from systems without a transition moment phase shift is the photorecombination time delay. Here, we use the group delay from a time-dependent Schrödinger equation (TDSE) simulation of a hydrogenic atom with an ionization potential of 15.8 eV (obtained by scaling the nuclear charge) as our reference, which has a slowly varying transition moment phase at large energies [30]. The difference between the measured group delay and the group delay from the simulation of the reference hydrogenic atom calculated with the experimental conditions represents the photorecombination time delay from our experimental measurement and is shown in Fig. 2C in red, and a smoothed version of the curve is shown in magenta. The maximum delay difference around the Cooper minimum near 54 eV is 180 as, in agreement with other studies of photorecombination time delays in argon [4]. The positive delay measured at energies below the Cooper minimum is similar to group delay from calculations of photoionization delays in argon [31] and results from the difference in the Coulomb scattering phase of the continuum states populated by the 1s and 3p orbitals of the reference hydrogenic and argon atoms, respectively [30].

While our results agree with previous measurements of the photorecombination time delay around the Cooper minimum in argon [4] and our own simulations of the experimental conditions, the energy region around the Cooper minimum lies within an energy range that could exhibit a signal contaminated by second-order diffraction of the high-energy components of our attosecond pulse spectra. We verified our measurement by filtering out the high-energy components of the attosecond pulse spectra, and our results remained consistent (details are discussed in the Supplementary Materials).

To support our experiment, we perform an ab initio simulation of an all-optical measurement in argon using TD-DFT [23]. The details of our implementation of TD-DFT are provided in the Supplementary Materials. We simulate the generation of an isolated attosecond pulse in argon using a single-cycle driving field with a wavelength of 1.8 μm and a peak intensity of $1 \times 10^{14}$ W/cm $^2$. We use an absorbing boundary [26], which begins at a radial distance of $0.8 \times F_0 / \omega_0^2$ in order to suppress emission from long trajectories and obtain a clear spectrum. We simulate an all-optical measurement by adding a weak second-harmonic of the driving field with a relative intensity of $10^{-4}$ and scanning the relative phase of the perturbing and driving fields. We do this for argon using TD-DFT and for a reference hydrogenic atom with the same ionization potential (15.8 eV) as the argon atom calculated with DFT and compare these results to isolate the effect of the transition moment phase on the all-optical measurement of attosecond pulse emission from argon.

The spectrogram from our simulated all-optical measurement is presented in Fig. 3A, which shows the variation of the attosecond pulse intensity spectrum with the relative phase between the driving and perturbing fields normalized for each emitted frequency. The overlaid solid red and dashed blue lines denote the phase that maximizes emission at each frequency from our simulated measurements in argon and the reference hydrogenic atom, respectively. Throughout the entire spectrum, the optimal relative phase from the argon and hydrogenic atom measurements increases with photon energy and plateaus near

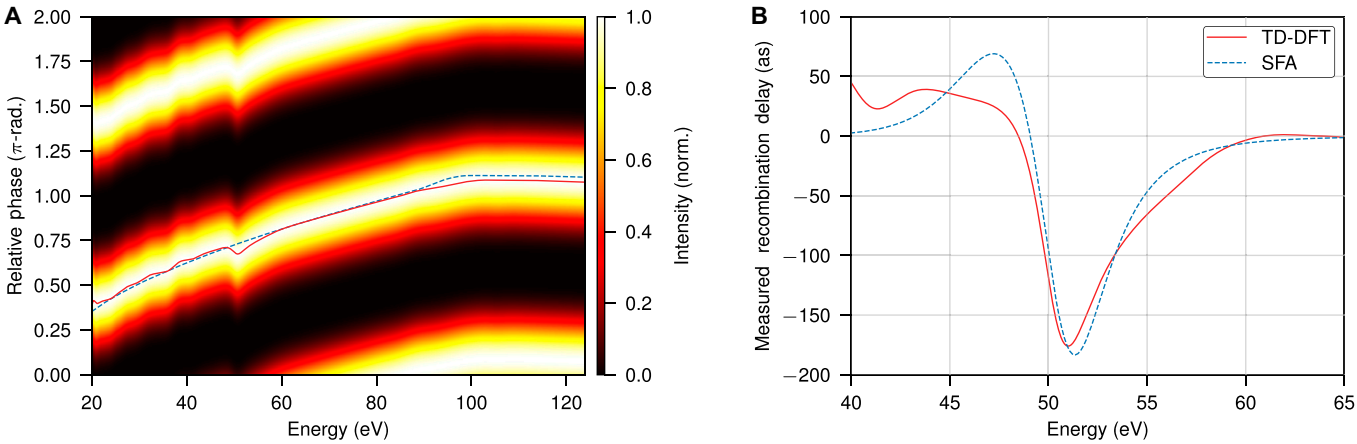


**Fig. 3.** Simulated all-optical measurement in argon. (A) Spectrogram from simulated $\omega - 2\omega$ all-optical measurement of attosecond pulse emission in argon calculated using time-dependent density functional theory. The overlaid red and blue lines denote the optimal relative phase between the driving and perturbing fields for each photon energy from all-optical measurements performed in argon and a reference hydrogenic atom with an equivalent ionization potential, respectively. (B) (Solid red) Difference between the optimal relative phase for the simulated all-optical measurements in argon calculated using TD-DFT and the reference hydrogenic atom. (Dashed blue) Change in the optimal relative phase in a model argon atom due to a Lorentzian $\pi$-phase shift in its recombination moment at 51 eV. The driving field is a single-cycle pulse with a wavelength of 1.8 μm and a peak intensity of $1 \times 10^{14}$ W/cm$^2$, the perturbing field is a second harmonic of the driving field with a relative intensity of $10^{-4}$, and absorbing boundaries [26] are used to suppress long trajectory emission.

100 eV, reflecting the conventional attochirp for short trajectory emission. Below 40 eV, the optimal phase from the argon measurement exhibits several modulations due to multi-channel and multi-pole effects [28].

At the Cooper minimum near 51 eV, the optimal phase from the argon measurement shows a clear modulation due to the transition moment phase shift. The difference between the optimal phase from the argon and reference hydrogenic atom around the Cooper minimum reveals how the transition moment phase shift around the Cooper minimum affects all-optical measurement. This is shown in Fig. 3B by the solid red curve. The dashed blue curve shows the difference between the measured group delay for an all-optical measurement from a model argon atom with a Lorentzian $\pi$-phase shift in its transition moment and a reference hydrogenic atom calculated using an extension of the SFA, which accounts for the transition moment phase shift in the calculation of recollision trajectories [21]. For the SFA calculation, the driving and perturbing fields are sinusoidal fields with the same respective wavelengths and peak intensities as in the TD-DFT calculation and only short trajectory emission is considered. A thorough description of the SFA and all-optical measurement for systems with a transition moment phase shift is provided in the Supplementary Materials.

Despite the comparatively simple model employed by the SFA, the difference in the measured group delay due to the transition moment phase from the TD-DFT simulation and the SFA calculation shows qualitative agreement. Both show positive variations in the measured group delay ~50 as at energies below the Cooper minimum and a maximum decrease in the measured group delay ~180 as at the Cooper minimum (51 eV). This agreement supports the inclusion of the transition moment phase in the calculation of recollision trajectories in the SFA.

Before discussing the implications of our work, we must first address the apparent contradiction of our results with previous works [16,17]. The first of these works [17] demonstrated theoretically that attosecond all-optical measurement is insensitive to the field-free transition moment phase due to the 2-center interference in a diatomic molecule. In order to obtain a sharp phase shift in the calculated HHG spectra, the first excited state was projected from simulations to reduce the polarizability of the ground state. This projection suppresses the influence of all external fields including the perturbing field used for measurement on the transition moment and forces the HHG spectrum to be shaped predominantly by the field-free transition moment similarly to the formalism suggested by QRS [18]. In contrast, our results necessarily include the full response of the system and the transition moment to all external fields. This is expounded upon in the Supplementary Materials.

The second of these works demonstrated attosecond all-optical techniques to be insensitive to transition moment phase shifts arising from a shape resonance in $SF_6$ [16]. The resolution of this disagreement lies in the distinct pathways to recombination in conventional recollision and recollision-induced shape resonance excitation. In the presence of a shape resonance, the continuum electron enters into a localized quasi-bound state prior to recombination to the ground state. The shape resonance in $SF_6$ has been shown to be robust against variations of external fields [32]. Thus, the quasi-bound state exhibits a much lower polarizability than the electron in the continuum and the influence of the perturbing field on the quasi-bound state is negligible when compared with that on the continuum electron. Consequently, the all-optical measurement of recollision in the presence of a shape resonance is sensitive only to the dynamics occurring prior to the excitation of the shape resonance, which are equivalent to those of conventional recollision. This is also expounded upon in the Supplementary Materials.

It is important to have a qualitative understanding of our results, for which we turn to the semiclassical model of recollision [1,3]. The sensitivity of the all-optical approach to the transition moment phase shift around the Cooper minimum in argon can be explained as a consequence of the spatial structure of the 3*p* orbital wavefunction. Cooper minima arise from a change in the sign of the dipole transition element with continuum state energy, resulting in a phase shift and spectral minimum in the transition moment [22].

Semiclassical recollision trajectories are calculated through the expression for the recollision dipole spectrum calculated using the SFA:

$$\widetilde{D}(\Omega) = -i\int_{-\infty}^{\infty} dt_r \int_{-\infty}^{t_r} dt_b \int dk \quad d_0^*\left(k + A(t_r)\right) e^{-iS(k,t_b,t_r) - iI_p(t_r - t_b)} F(t_b) d_0\left(k + A(t_b)\right), \tag{2}$$

where $I_p$ is the ionization potential, $A(t)$ and $F(t)$ are the driving field vector potential and electric field at time $t$, $d_0(k)$ is the transition moment between the ground state and continuum state with momentum $k$, and $S(k, t_b, t_r)$ is the semiclassical action. We let $\eta(k)$ denote the phase of the transition moment:

$$\eta(k) = \arg\left(d_0(k)\right). \tag{3}$$

Equation 3 is typically solved using saddle-point integration, which involves finding and setting the derivatives of the integrand phase with respect to the integration variables to zero, resulting in a system of equations whose solutions correspond to the dominant contributions of the integrand. The equation obtained from the evaluating derivative of the integrand phase in Eq. 3 with respect to $k$, which is broadly interpreted as a displacement condition for recollision trajectories, including the transition moment phase is given as follows [21]:

$$0 = \int_{t_b}^{t_r} \left[k + A(\tau)\right] d\tau + \eta'\left(k + A\left(t_b\right)\right) - \eta'\left(k + A\left(t_r\right)\right), \tag{4}$$

where $\eta'(k)$ is the gradient of the transition moment phase at momentum $k$. The integration of the kinetic momentum between times $t_b$ and $t_r$ describes the displacement of the recollision electron due to the driving field. For the case of a slowly varying transition moment phase, $|\eta'(k)| \sim 0$ and Eq. 4 states that a recollision electron must return to its position of origin to undergo recollision. When the transition moment phase varies sufficiently rapidly, the second and third terms act as momentum-dependent spatial offsets of the relative positions of ionization and recombination. While the dynamics of recollision and recombination are inherently quantum mechanical and wave-like in nature, the interpretation of Eq. 5 as a displacement condition for semiclassical trajectories and the localization of ionization and recombination during recollision have led to many valuable insights [8–11,33–37], which we extend here.

If we consider the Cooper minimum in argon, the semiclassical interpretation of Eq. 5 is clear: As the recollision electron kinetic energy passes through the Cooper minimum, the displacement condition in Eq. 5 requires that the difference between the positions of ionization and recombination changes according to the gradient of the transition moment phase around the Cooper

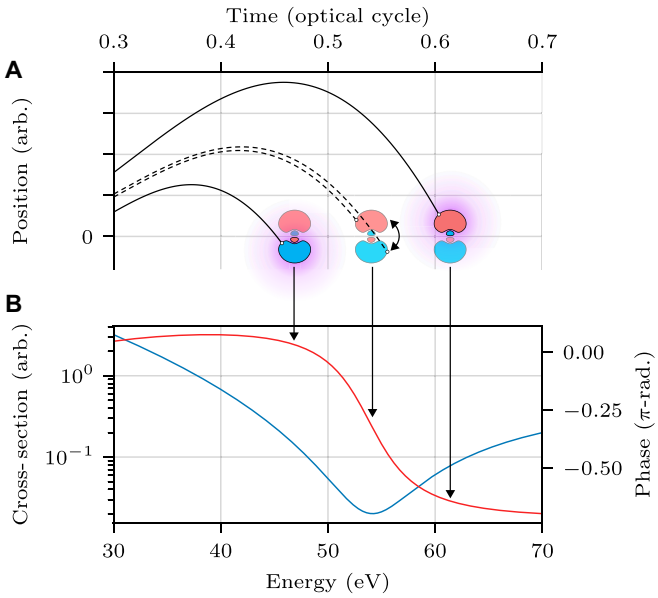


**Fig. 4.** Qualitative depiction of recollision in argon. (A) Recollision trajectories leading to photon emission in argon and (B) the transition moment cross-section (blue, left axis) and phase (red, right axis) in argon. The trajectories in (A) leading to photon emission at a given energy in (B) are denoted by the black vertical arrows. In (A), the $3p_0$ orbital in Ar is overlaid for each trajectory at the time of recombination, denoting the position of recombination with the white circles and the orbital lobe that dominates dipole emission as originally described by Cooper. At energies below (above) the Cooper minimum, the lower (upper) lobe dominates dipole emission. Around the Cooper minimum, the lobe that dominates dipole emission changes, as denoted by the dashed trajectories and the double-headed arrow.

minimum. This is depicted in Fig. 4, which shows a qualitative depiction of recollision trajectories as a function of time in (A) and the cross-section (blue, left axis) and transition moment phase (red, right axis) of argon in (B). Due to the linear atto-chirp, the recombination time of a given trajectory can be mapped to an emitted photon energy and this energy is denoted by the vertical black arrows relating Fig. 4A and B. For a recollision trajectory leading to photon emission below (above) the Cooper minimum, the position of recombination is the lower (upper) lobe of the $3p_0$ orbital. The position of recombination is depicted by the white circles and purple hue, representing XUV emission. At the Cooper minimum, the position of recombination shifts from one lobe to the other as the radial dipole matrix element changes sign [22], resulting in the variation of recollision dynamics as observed in our experiment.

This interpretation is closely related to the localization of ionization and recombination in the molecular SFA [33], where the outer lobes of the $3p_0$ orbital play the role of distinct atomic centers in the linear combination of atomic orbital description of molecular systems. As a first-order approximation, the distance traveled by an electron traveling with the kinetic energy leading to photon emission at 54 eV during a time of 180 as is 12 a.u. (atomic units), roughly the spatial extent of the $3p_0$ orbital. A more thorough description of the semiclassical interpretation is provided in a related paper [21].

## Conclusion

To conclude, we have experimentally verified the predictions of our previous work [21], which argued that the recollision electron wave packet when observed through attosecond pulse emission is not independent of the transition moment phase. We now stand back even further from the details of the current experiment and consider the close connection between nonlinear optics and photoionization time delay measurements in attosecond physics. Nonlinear optics requires that the nonlinear process, whether perturbative or nonperturbative, returns the system to its initial or a coherently related state. If this were not the case, phase matching would be impossible. In other words, the 3-step recollision model requires that photoionization and photorecombination are identical—the recolliding wave packet that produces a pulse is identical to the outgoing wave packet created by that pulse.

In support of this general principle, we have demonstrated the link between recollision trajectories and the transition moment phase by measuring the photorecombination time delay around the Cooper minimum in argon entirely optically. Compared with traditional forms of attosecond measurement based on photoionization [5,6] that require a sophisticated photoelectron spectrometer in addition to the attosecond pulse generation apparatus [38], optical measurements are much easier to accomplish. Our all-optical approach can be readily generalized to studying multielectron interaction including collision-induced plasma excitation [39,40] and Fano resonances [41] and can be extended to gas-phase molecules [42] and possibly solids [43]. Further, our results suggest a form of electron orbital tomography, wherein the spatial structure of a wavefunction can be inferred from all-optical measurements of recollision. This is expounded upon in a related study, which considers the effect of the transition moment phase using the SFA [3,21].

Assessing these differing measurement approaches, measuring time delays by photoionization is encumbered by their sensitivity to many possible sources of delay, including electron dynamics [42], molecular structure [44], and dispersive effects during attosecond pulse propagation [7], leading to a lack of clarity regarding the measurement. In contrast, our all-optical measurement is sensitive to the transition moment phase around the Cooper minimum in argon and is predicted to be insensitive to field-free ionic structure [21]. Other collinear all-optical measurement techniques have been shown to be insensitive to 2-center interference and shape resonances [16,17]. Since photoionization and photorecombination experiments measure different things, combining them will allow us to unambiguously isolate the time delays associated with molecular structural and electron dynamic effects.

Finally, trajectory dynamics and recombination have typically been treated as independent [18]. The sensitivity of our all-optical approach, however, demonstrates the limitations of this approximation. The recollision electron wave packet, as observed through the recollision dipole moment, is not independent of its parent ion. Our results have significant implications regarding how recollision is described on a fundamental level. In particular, the independence of continuum electron wave packet when observed through attosecond pulse emission and the generation medium has been used to justify theoretical descriptions of attosecond pulse generation [18] and the interpretation of experimental measurements. Our results show that the assumption that recollision trajectories are independent of the transition moment phase is an approximation. The interdependence of recollision trajectories and the source medium must be addressed in the interpretation of all attosecond experiments. This has already been understood in the

context of solid-state HHG [45], and limitations of QRS have been identified in other gas-phase experimental works [33,46]. Our results clearly demonstrate the limitations of treating recollision trajectories and recombination as independent processes and will pave the way for more efficient measurements of ultrafast electron dynamics in atomic, molecular, and solid-state systems.

## Acknowledgments

**Funding:** This research was supported by the United States Air Force Office of Scientific Research (award no. FA9550-16-1-0109) with contributions from the Canada Foundation for Innovation, the Canada Research Chairs Program, Canada's Natural Sciences and Engineering Research Council, and the National Research Council of Canada. **Author contributions:** C.Z. and D.H.K. designed the experiment. C.Z. performed the experiment. G.B. performed the numerical and semiclassical theoretical analysis and interpreted the experimental results. G.B. and C.Z. analyzed the experimental data. G.B. and P.B.C. prepared the initial manuscript. All authors contributed in writing the manuscript. C.Z. and P.B.C. supervised the work. **Competing interests:** The authors declare that they have no competing interests.

## Data Availability

The data that support the findings of this study are available from the corresponding authors upon reasonable request.

## Supplementary Materials

Supplementary Text
Figs. S1 to S11
References [47–52]

## References

1. Corkum PB. Plasma perspective on strong field multiphoton ionization. *Phys Rev Lett*. 1993;71:1994.
2. Varjú K, Mairesse Y, Carré B, Gaarde MB, Johnsson P, Kazamias S, López-Martens R, Mauritsson J, Schafer KJ, Balcou PH, et al. Frequency chirp of harmonic and attosecond pulses. *J Mod Opt*. 2005;52:379–394.
3. Lewenstein M, Balcou P, Ivanov MY, L'Huillier A, Corkum PB. Theory of high-harmonic generation by low-frequency laser fields. *Phys Rev A*. 1994;49:2117.
4. Schoun SB, Chirla R, Wheeler J, Roedig C, Agostini P, DiMauro LF, Schafer KJ, Gaarde MB. Attosecond pulse shaping around a cooper minimum. *Phys Rev Lett*. 2014;112:153001.
5. Paul PM, Toma ES, Breger P, Mullot G, Augé F, Balcou P, Muller HG, Agostini P. Observation of a train of attosecond pulses from high harmonic generation. *Science*. 2001;292:1689.
6. Itatani J, Quéré F, Yudin GL, Ivanov MY, Krausz F, Corkum PB. Attosecond streak camera. *Phys Rev Lett*. 2002;88:173903.
7. Cattaneo L, Vos J, Lucchini M, Gallmann L, Cirelli C, Keller U. Comparison of attosecond streaking and rabbitt. *Opt Express*. 2016;24:29060.
8. Dudovich N, Smirnova O, Levesque J, Mairesse Y, Ivanov MY, Villeneuve DM, Corkum PB. Measuring and controlling the birth of attosecond xuv pulses. *Nat Phys*. 2006;2:781.
9. Kim KT, Villeneuve DM, Corkum PB. Manipulating quantum paths for novel attosecond measurement methods. *Nat Photonics*. 2014;8:187.
10. Kim KT, Zhang C, Shiner AD, Kirkwood SE, Frumker E, Gariepy G, Naumov A, Villeneuve DM, Corkum PB. Manipulation of quantum paths for space–time characterization of attosecond pulses. *Nat Phys*. 2013;9:159.
11. Ko DH, Brown GG, Zhang C, Corkum PB. Near-field imaging of dipole emission modulated by an optical grating. *Optica*. 2021;8:1632.
12. Vampa G, Hammond TJ, Thiré N, Schmidt BE, Légaré F, McDonald CR, Brabec T, Klug DD, Corkum PB. All-optical reconstruction of crystal band structure. *Phys Rev Lett*. 2015;115:193603.
13. Zhang C, Brown GG, Kim KT, Villeneuve DM, Corkum PB. Full characterization of an attosecond pulse generated using an infrared driver. *Sci Rep*. 2016;6:26771.
14. Bruner BD, Mašín Z, Negro M, Morales F, Brambila D, Devetta M, Faccialà D, Harvey AG, Ivanov M, Mairesse Y, et al. Multidimensional high harmonic spectroscopy of polyatomic molecules: Detecting sub-cycle laser-driven hole dynamics upon ionization in strong mid-ir laser fields. *Faraday Discuss*. 2016;194:369.
15. Pedatzur O, Orenstein G, Serbinenko V, Soifer H, Bruner BD, Uzan AJ, Brambila DS, Harvey AG, Torlina L, Morales F, et al. Attosecond tunnelling interferometry. *Nat Phys*. 2015;11:815.
16. Orenstein G, Pedatzur O, Uzan AJ, Bruner BD, Mairesse Y, Dudovich N. Isolating strong-field dynamics in molecular systems. *Phys Rev A*. 2017;95:051401.
17. Spanner M, Bertrand JB, Villeneuve DM. In situ attosecond pulse characterization techniques to measure the electromagnetic phase. *Phys Rev A*. 2016;94:023825.
18. Le A-T, Lucchese RR, Tonzani S, Morishita T, Lin CD. Quantitative rescattering theory for high-order harmonic generation from molecules. *Phys Rev A*. 2009;80:013401.
19. Farrell JP, Spector LS, McFarland BK, Bucksbaum PH, Gühr M, Gaarde MB, Schafer KJ. Influence of phase matching on the cooper minimum in ar high-order harmonic spectra. *Phys Rev A*. 2011;83:023420.
20. Itatani J, Levesque J, Zeidler D, Niikura H, Pépin H, Kieffer JC, Corkum PB, Villeneuve DM. Tomographic imaging of molecular orbitals. *Nature*. 2004;432:867.
21. Brown GG, Ko DH, Zhang C, Corkum PB. Attosecond measurement via high-order harmonic generation in low-frequency fields. *Phys Rev A*. 2022;105:023520.
22. Cooper JW. Photoionization from outer atomic subshells. A model study. *Phys Rev*. 1962;128:681.
23. Maitra NT. Perspective: Fundamental aspects of time-dependent density functional theory. *J Chem Phys*. 2016;144:220901.
24. Oron D, Silberberg Y, Dudovich N, Villeneuve DM. Efficient polarization gating of high-order harmonic generation by polarization-shaped ultrashort pulses. *Phys Rev A*. 2005;72:063816.
25. Flettner A, König J, Mason MB, Pfeifer T, Weichmann U, Düren R, Gerber G. Ellipticity dependence of atomic and molecular high harmonic generation. *Eur Phys J D At Mol Opt Phys*. 2002;21:115–119.
26. Manolopoulos DE. Derivation and reflection properties of a transmission-free absorbing potential. *J Chem Phys*. 2002;117:9552.

27. Telnov DA, Sosnova KE, Rozenbaum E, Chu S-I. Exterior complex scaling method in time-dependent density-functional theory: Multiphoton ionization and high-order-harmonic generation of ar atoms. *Phys Rev A*. 2013;87:053406.
28. Pabst S, Greenman L, Mazziotti DA, Santra R. Impact of multichannel and multipole effects on the cooper minimum in the high-order-harmonic spectrum of argon. *Phys Rev A*. 2012;85:023411.
29. Higuet J, Ruf H, Thiré N, Cireasa R, Constant E, Cormier E, Descamps D, Mével E, Petit S, Pons B, et al. High-order harmonic spectroscopy of the cooper minimum in argon: Experimental and theoretical study. *Phys Rev A*. 2011;83:053401.
30. Popruzhenko SV. Coulomb phase in high harmonic generation. *J Phys B Atomic Mol Phys*. 2018;51:144006.
31. Pi L-W, Landsman AS. Attosecond time delay in photoionization of noble-gas and halogen atoms. *Appl Sci*. 2018;8:322.
32. Manschwetus B, Lin N, Rothhardt J, Guichard R, Auguste T, Camper A, Breger P, Caillat J, Géléoc M, Ruchon T, et al. Self-probing spectroscopy of the sf6 molecule: A study of the spectral amplitude and phase of the high harmonic emission. *Chem A Eur J*. 2015;119:6111.
33. Labeye M, Risoud F, Lévêque C, Caillat J, Maquet A, Shaaran T, Salières P, Taïeb R. Dynamical distortions of structural signatures in molecular high-order harmonic spectroscopy. *Phys Rev A*. 2019;99:013412.
34. Suárez N, Chacón A, Pérez-Hernández JA, Biegert J, Lewenstein M, Ciappina MF. High-order-harmonic generation in atomic and molecular systems. *Phys Rev A*. 2017;95:033415.
35. Chirilă CC, Lein M. Strong-field approximation for harmonic generation in diatomic molecules. *Phys Rev A*. 2006;73:023410.
36. Figueira de Morisson Faria C. High-order harmonic generation in diatomic molecules: A quantum-orbit analysis of the interference patterns. *Phys Rev A*. 2007;76:043407.
37. Etches A, Gaarde MB, Madsen LB. Two-center minima in harmonic spectra from aligned polar molecules. *Phys Rev A*. 2011;84:023418.
38. Hentschel M, Kienberger R, Spielmann C, Reider GA, Milosevic N, Brabec T, Corkum P, Heinzmann U, Drescher M, Krausz F. Attosecond metrology. *Nature*. 2001;414:509.
39. Shiner AD, Schmidt BE, Trallero-Herrero C, Wörner HJ, Patchkovskii S, Corkum PB, Kieffer JC, Légaré F, Villeneuve DM. Probing collective multi-electron dynamics in xenon with high-harmonic spectroscopy. *Nat Phys*. 2011;7:464.
40. Pabst S, Santra R. Strong-field many-body physics and the giant enhancement in the high-harmonic spectrum of xenon. *Phys Rev Lett*. 2013;111:233005.
41. Strelkov VV, Khokhlova MA, Shubin NY. High-order harmonic generation and fano resonances. *Phys Rev A*. 2014;89:053833.
42. Biswas S, Förg B, Ortmann L, Schötz J, Schweinberger W, Zimmermann T, Pi L, Baykusheva D, Masood HA, Liontos I, et al. Probing molecular environment through photoemission delays. *Nat Phys*. 2020;16:778.
43. Silva REF, Blinov IV, Rubtsov AN, Smirnova O, Ivanov M. High-harmonic spectroscopy of ultrafast many-body dynamics in strongly correlated systems. *Nat Photonics*. 2018;12:266.
44. Vozzi C, Calegari F, Benedetti E, Berlasso R, Sansone G, Stagira S, Nisoli M, Altucci C, Velotta R, Torres R, et al. Probing two-centre interference in molecular high harmonic generation. *J Phys B Atomic Mol Phys*. 2006;39:S457.
45. Jiang S, Wei H, Chen J, Yu C, Lu R, Lin CD. Effect of transition dipole phase on high-order-harmonic generation in solid materials. *Phys Rev A*. 2017;96:053850.
46. Faccialà D, Pabst S, Bruner BD, Ciriolo AG, Devetta M, Negro M, Geetha PP, Pusala A, Soifer H, Dudovich N, et al. High-order harmonic generation spectroscopy by recolliding electron caustics. *J Phys B Atomic Mol Phys*. 2018;51:134002.
47. Wang J, Chu S-I, Laughlin C. Multiphoton detachment of $H^-$. II. intensity-dependent photodetachment rates and threshold behavior—Complex-scaling generalized pseudospectral method. *Phys Rev A*. 1994;50:3208–3215.
48. Jackson JD. *Classical electrodynamics*. 3rd ed. New York (NY): Wiley; 1999.
49. van Leeuwen R, Baerends EJ. Exchange-correlation potential with correct asymptotic behavior. *Phys Rev A*. 1994;49:2421.
50. Bauer D (Ed). *Computational strong-field quantum dynamics* Berlin, Boston: De Gruyter; 2017.
51. Śpiewanowski MDS, Etches A, Madsen LB. High-order-harmonic generation from field-distorted orbitals. *Phys Rev A*. 2013;87:043424.
52. Śpiewanowski MDS, Madsen LB. Field-induced orbital distortion in high-order-harmonic generation from aligned and oriented molecules within adiabatic strong-field approximation. *Phys Rev A*. 2014;89:043407.